PCCP

Accepted Manuscript

ROYAL SOCIETY OF CHEMISTRY

www.rsc.org/pccp

Cite this: DOI: 10.1039/c0xx00000x

www.rsc.org/xxxxxx

ARTICLE TYPE

Bi-overlayer Type Plasmonic Photocatalyst Consisting of Mesoporous Au/TiO_2 and CuO/SnO_2 Films Separately Coated on FTO

Shin-ichi Naya,[a] Takahiro Kume,[b] Nozomi Okumura [b] and Hiroaki Tada* [a,b]

Received (in XXX, XXX) Xth XXXXXXXXX 20XX, Accepted Xth XXXXXXXXX 20XX

DOI: 10.1039/b000000x

The principal purpose of this study is to present a new design for preparing highly active immobilized gold nanoparticle-based plasomnic photocatalysts. Gold nanoparticles were loaded on rutile TiO_2 particles with a mean size of 80 nm (Au/TiO_2) by the deposition precipitation method. The surface of SnO_2 particles with a mean size of 100 nm was modified by copper(II) oxide clusters (CuO/SnO_2) with the loading amount (Γ/Cu ions nm^{-2}) precisely controlled by the chemisorption-calcination cycle technique. Two mesoporous overlayers of Au/TiO_2 and CuO/SnO_2 were coated side by side on glass substrates with a fluorine-doped tin oxide film (FTO) using the doctor blade method (Au/mp-TiO_2 | FTO | CuO/mp-SnO_2). As test reactions for assessing the visible-light activity, we carried out gas-phase decomposition of acetaldehyde and liquid-phase oxidation of alcohol. In each reaction, this bi-overlayer type catalyst shows a high level of visible-light activity much exceeding those of Au/TiO_2 particles and a Au/mp-TiO_2 | FTO mono-overlayer type catalyst [*J. Phys. Chem. C* **2014**, *118*, 26887]. To clarify the origin for the striking visible-light activity, we studied the electrocatalytic activity of CuO/mp-SnO_2 | FTO electrodes for the oxygen reduction reaction (ORR). Both the visible-light activity of Au/mp-TiO_2 | FTO | CuO/mp-SnO_2 and the electrocatalytic activity of CuO/mp-SnO_2 | FTO for ORR strongly depend on the Γ value. A good positive correlation has been found between the visible-light activities and the electrocatalytic activity for ORR. The striking activity of the present bi-overlayer type catalyst can be attributed to the efficient and long-range charge separation by the vectrial electron transport (Au(oxidation sites) → TiO_2 → FTO, SnO_2 → CuO(reduction sites)) and the excellent electrocatalytic activity of the CuO clusters.

1 INTRODUCTION

The efficient sunlight utilization for the organic synthetic process and the air and water purification would greatly contribute to the dissolution of the energy and environmental issues. To this end, a highly active visible-light catalyst must be developed because the energy of visible light occupies 45% of the total solar energy. Besides the semiconductors mainly studied so far, gold nanoparticles with strong absorption in a wide visible region due to the localized surface plasmon resonance (LSPR) is a promising candidate for the inductor of the visible-light-driven chemical reactions.[1-3] Recently, gold nanoparticle-loaded metal oxides such as titanium dioxide (Au/MOs) have emerged as a new type of visible-light photocatalysts, the so-called "plasmonic photocatalysts".[4-6] The LSPR-excitation of Au/TiO_2 gives rise to the interfacial electron transfer from Au nanoparticles to the conduction band (CB) of TiO_2.[7,8] As a result of the lowering in the Fermi energy, oxidation can take place on the surface of Au nanoparticles, while O_2 is reduced by the CB(TiO_2) electrons. So far, particulate Au/TiO_2 plasmonic photocatalysts have been applied for environmental remediation [9,10] and several oxidative transformations including alcohol to carbonyl compounds,[11-14] thiol to disulfide,[15] benzene to phenol,[16,17] and amine to imine.[18] However, the electrons injected into the CB(TiO_2) undergo the rapid back electron transfer lowering the activity.[19] The key to increasing the activity is the enhancement of the charge separation for the photogenerated charge carriers to be effectively

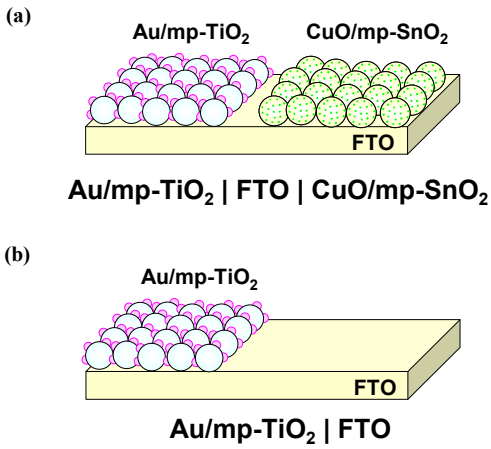

Scheme 1. Bi-overlayer (a) and mono-overlayer (b) type plasmonic photocatalysts.

used for surface reactions. We have reported that Au/TiO_2 with a bimodal size distribution of Au nanoparticles exhibits a high level of activity for the one-step synthesis of azobenzenes from nitrobenzenes with high yield and selectivity because of the electron transport from small Au nanoparticles to large ones.[20] As other approaches to enhance the charge separation, Ide *et al.* have hybridized Au/TiO_2 with boron nitride,[21] and Tachikawa and Majima *et al.* have used an advanced superstructure TiO_2 as the support of Au nanoparticles in the place of TiO_2 particles.[22] More recently, we have shown that the immobilization of Au/TiO_2 on conducting substrates (Au/mp-TiO_2 | conducting material underlayer) causes the efficient interfacial electron transfer from the Au/TiO_2 overlayer to the conducting underlayer, remarkably improving the visible-light activity as compared to Au/TiO_2.[23] Another point is the enhancement of the O_2 reduction, which can be frequently the rate-determining step in the photocatalytic reactions. In the preceding work,[23] we have found that the Au/mp-TiO_2 | Pt shows the highest photocatalytic activity among Au/mp-TiO_2 on various conducting substrates.[23] Regardless of the high cost, Pt is usually used as the cathode of fuel cells due to its excellent electrocatalyst for oxygen reduction reaction (ORR).[24] The application of the large-scale fuel cells needs the development of Pt-alternative materials with high electrocatalytic activity for ORR, low cost, and earth abundance. Recently, the surface modification of TiO_2 with copper(II) oxide clusters by the chemisorption-calcination cycle (CCC) technique has been reported to enhance ORR.[25]

We coated two mesoporous films consisting of Au/TiO_2 particles and CuO/SnO_2 particles side by side on one FTO substrate (Au/mp-TiO_2 | FTO | CuO/mp-SnO_2). In Scheme 1, the structure is shown by comparison with the structure of a mono-overlayer type catalyst (Au/mp-TiO_2 | FTO). This bi-overlayer type photocatalyst is expected to be applicable for gas-phase reactions as well as liquid-phase reactions since it does not need external bias and electrolyte solution. We studied the removal and decomposition of gaseous acetaldehyde as a gas-phase test reaction. Among pollutants in the room air, acetaldehyde is a prevailing volatile organic compound responsible for the sick-house syndrome. On the other hand, the oxidation of alcohol to aldehyde is one of the key reactions in the organic synthesis, and the development of the "green processes" using O_2 as an oxidizing agent is highly desired. Thus, the partial oxidation of alcohol as a liquid-phase test reaction.

2 EXPERIMENTAL

2.1 Preparation and characterization of mesoporous film of Au/TiO_2 on FTO (Au/mp-TiO_2 | FTO).

Au particles were loaded on rutile TiO_2 particles with a specific surface area of 17.5 m^2 g^{-1} (MT-700B, TAYCA, mean particle size = 80 nm) by the deposition–precipitation (DP) method using $HAuCl_4$ as a starting material.[26,27] The post-heating was carried out at 500 °C for 4 h. A slurry of Au/TiO_2 (0.5 g) in H_2O (1 mL) with acetylacetone (50 mg), Triton X (0.25 mL) and polyethylene glycol 20000 (0.25 g) was coated on fluorine-doped thin oxide film (FTO, sheet resistance = 12 Ω/square). The paste coated samples were heated in air at 500 °C for 1 h to form Au/mp-TiO_2. The mean size of the Au nanoparticles was determined by transmission electron microscopy at an applied voltage of 300 kV (JEM-3010, JEOL). The film thickness and morphologies were examined by scanning electron microscopy (SEM, Hitachi S-800) at an acceleration voltage of 15 kV. The Au loading amount was quantified by inductively coupled plasma spectroscopy (ICPS-7500, Shimadzu). Diffuse reflectance UV-Vis-NIR spectra of the samples were recorded on a Hitachi U-4000 spectrometer mounted with an integrating sphere at room temperature. The reflectance (R_∞) was recorded with respect to a reference of $BaSO_4$, and the Kubelka-Munk function [$F(R_\infty)$] expressing the relative absorption coefficient was calculated by the equation $F(R_\infty) = (1 - R_\infty)^2/2R_\infty$.

2.2 Preparation and characterization of mesoporous film of copper oxide cluster-surface modified SnO_2 on FTO.

Copper oxide clusters were loaded on the surface of SnO_2 particles with a specific surface area of 8.6 m^2 g^{-1} (Aldrich, mean particle size = 100 nm) by the chemisorption-calcination-cycle (CCC) method.[25,28] SnO_2 particles (2 g) were suspended in MeOH solution (50 mL) of $Cu(acac)_2$ with various concentration, and they were allowed to stand for 18 h at 298 K in dark. The $Cu(acac)_2$ concentration was changed from 0.1 to 5.0 mM. Particles were corrected by centrifugation, and washed with MeOH three times. After drying in vacuo, the resulting particles were calcined at 773 K for 1 h to yield CuO/SnO_2. A slurry of CuO/SnO_2 (0.5 g) in H_2O (1 mL) with acetylacetone (50 mg), Triton X (0.25 mL) and polyethylene glycol 20000 (0.25 g) was coated on FTO (sheet resistance = 12 Ω/square). The paste coated samples were heated in air at 500 °C for 1 h to form CuO/mp-SnO_2. The film thickness and morphologies were examined by scanning electron microscopy (SEM, Hitachi S-800) at an acceleration voltage of 15 kV. The Cu loading amount was quantified by inductively coupled plasma spectroscopy (ICPS-7500, Shimadzu). Diffuse reflectance UV-Vis-NIR spectra of the samples were recorded on a Hitachi U-4000 spectrometer mounted with an integrating sphere at room temperature. The reflectance (R_∞) was recorded with respect to a reference of $BaSO_4$, and the Kubelka-Munk function [$F(R_\infty)$] expressing the relative absorption coefficient was calculated by the equation $F(R_\infty) = (1 - R_\infty)^2/2R_\infty$. X-ray photoelectron spectroscopic (XPS) measurements were performed using a Kratos Axis Nova X-ray photoelectron spectrometer with a monochromated Al Kα X-ray source operated at 15 kV and 10 mA using C1s as the energy reference (284.6 eV).

2.3 Au/TiO_2-photocatalyzed decomposition of gaseous acetaldehyde.

A reaction chamber (0.64 L) with Au/mp-TiO_2 (16 cm^2) | FTO | CuO/mp-SnO_2 (8 cm^2), Au/mp-TiO_2 (16 cm^2) | FTO, Au/mp-TiO_2 (16 cm^2) | glass, or Au/TiO_2 particles (16 mg) placed was evacuated by a rotary vacuum pump, and then a nitrogen-balanced acetaldehyde gas (516 ppm) was introduced to be diluted to ~100 ppm with air. After exposing catalyst to the gas at 298 K in dark for 2 h, visible light was irradiated for 24 h using a 300 W Xe lamp (HX-500, Wacom) with a cut off filter Y-45 (AGC TECHNO GLASS). The light intensity integrated from 420 to 485 nm ($I_{420–485}$) through a Y-45 optical filter was adjusted to 3.0 mW cm^{-2}. The concentration of acetaldehyde was determined by Gas chromatography (GC-2014 with methanizer MTN-1, C-R8A (Shimadzu)) [measurement conditions: column =

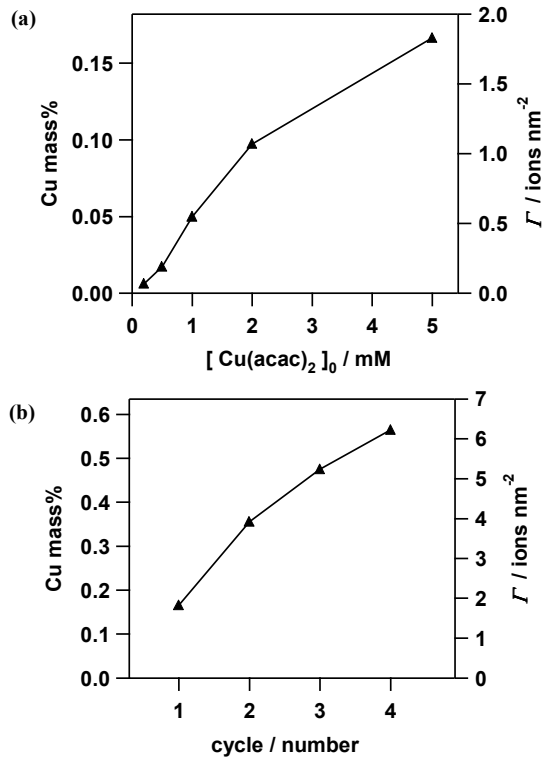

Fig. 1. Plots of copper loading amount as a function of the initial $Cu(acac)_2$ concentration ($[Cu(acac)_2]_0$) (a) and CC cycle number (N) at $[Cu(acac)_2]_0$ = 5 mM (b).

Porapak-Q 80-100 (GL science); N_2 flow rate = 50 mL min^{-1}].

2.4 Au/TiO_2-photocatalyzed oxidation of cinnamyl alcohol.

After Au/mp-TiO_2 (4 cm^2) | FTO | CuO/mp-SnO_2 (4 cm^2) or Au/mp-TiO_2 (4 cm^2) | FTO had been added to aqueous solution of cinnamyl alcohol (500 μM, 20 mL) and placed at 298 K in dark for 1 h, irradiation was started using a 300 W Xe lamp (HX-500, Wacom) with a cut off filter Y-45 (AGC TECHNO GLASS) in a double jacket type reaction cell. The cell was kept at a given temperature by circulating thermostated water through an outer jacket around the cell. The light intensity integrated from 420 to 485 nm ($I_{420–485}$) through a Y-45 optical filter was adjusted to 6.0 mW cm^{-2}. The yield and selectivity determined by UV/Vis spectroscopy (UV-1800, Shimadzu).

2.5 Electrochemical measurements for the evaluation of the electrocatalytic activity for O_2 reduction.

The electrochemical properties of the CuO/mp-SnO_2 (4 cm^2) | FTO electrodes were measured in 0.1 M $NaClO_4$ aqueous solution in a regular three-electrode electrochemical cell using a galvanostat/potentiostat (HZ-5000, Hokuto Denko). Glassy carbon and a Ag/AgCl electrode (TOA-DKK) were used as a counter electrode and a reference electrode, respectively.

3 RESULTS AND DISCUSSION

3.1 Preparation and characterization of Au/mp-TiO_2 | FTO

Au/TiO_2 particles were synthesized by the deposition-precipitation method.[26,27] Fig. S1 in Electronic Supporting Infomation (ESI) shows a TEM image of Au/TiO_2 particles (a) and the Au particle size distribution (b). Fairly uniform Au nanoparticles were highly dispersed on the TiO_2 surface. A Au/TiO_2 paste was parepared by dispersing Au/TiO_2 particles into an aqueous solution containing acetylacetone, Triton X, and polyethylene glycol 20000. The paste layer (thickness ≈ 25 μm and area = 16 or 4 cm^2) was formed on the substrates by the doctor blade technique. Post-heating of the sample in air at 500 °C for 1 h yielded mesoporous Au/TiO_2 films on FTO (Au/mp-TiO_2 | FTO) and glass substrates (Au/mp-TiO_2 | glass). Fig. S2a in ESI shows a cross-sectional SEM image of Au/mp-TiO_2 | FTO. A mesoporous Au/TiO_2 film with thickness of ~ 5 μm is formed on the FTO film. Fig. S2b shows the UV-Vis absorption spectra of Au/TiO_2 particles, Au/mp-TiO_2 | FTO, and Au/mp-TiO_2 | glass. For clarity, the spectra of the film samples are shown with shifted towards the upper side. Au/TiO_2 has a broad absorption around 570 nm due to the LSPR of Au nanoparticles. The peak position and shape of the LSPR absorption band are sensitive to the Au particle size and morphology.[1-3] The resemblance of the spectral shapes between the original particles and the resulting films on the substrates indicates that the size and morphology of Au nanoparticles remain after the film formation.

3.2 Preparation and characterization of CuO/mp-TiO_2 | FTO

The surface of SnO_2 particles was modified with copper oxides by the CCC method.[25,28] SnO_2 particles were suspended to $Cu(acac)_2$ solution, and they were allowed to stand for 18 h at

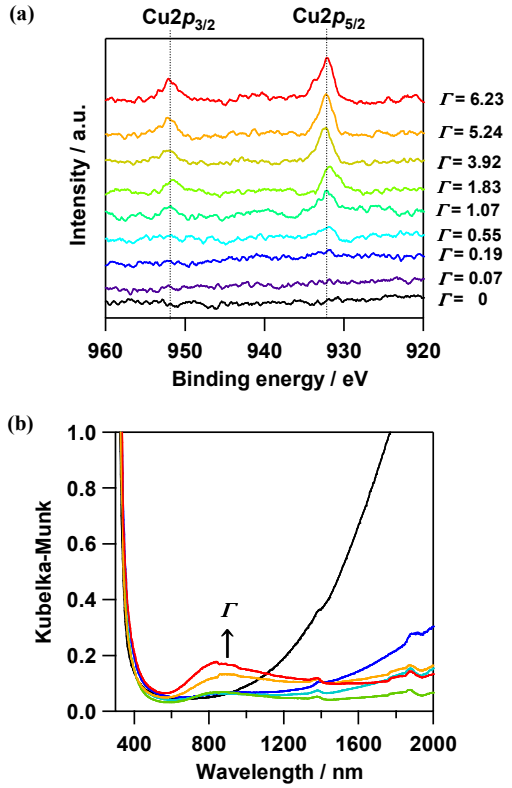

Fig. 2. (a) Cu 2*p*-XPS spectra for the CuO/SnO_2 with varying CuO loading (Γ). (b) UV-Vis-NIR absorption spectra of the CuO/SnO_2 with varying CuO loading (Γ).

298 K for the adsorption. After washing out the physisorbed complexes, the resulting particles were calcined at 773 K for 1 h to yield the copper oxide-loaded SnO_2. The copper loading amount was expressed by mass percent (mass%) and the number of copper ions per unit surface area of SnO_2 (Γ/ions nm^{-2}). Fig. 1 shows copper loading amount as a function of the initial $Cu(acac)_2$ concentration ($[Cu(acac)_2]_0$) (a) and CC cycle number (N) at $[Cu(acac)_2]_0$ = 5 mM (b). The Γ increases with an increase in $[Cu(acac)_2]_0$ and N. Clearly, the Cu loading amount can be precisely controlled by the $[Cu(acac)_2]_0$ at $\Gamma < \sim 2$ and by N at $\Gamma > \sim 2$ in the CCC technique.

To examine the oxidation state of the copper on the SnO_2 surface, the X-ray photoelectron spectroscopic (XPS) measurements were performed. Fig. 2a shows the Cu2p XPS spectra for the copper oxide surface-modified SnO_2 with varying Γ. The signals are observed at the binding energy = 932.1 and 951.9 eV assignable to the emission from the Cu2p5/2 and Cu2p3/2 orbitals, respectively. The presence of the weak satellite peak around 940 eV suggests that the oxidation number of copper ions is +2. Further, UV-visible absorption spectra of the samples were measured. Fig. 2b shows UV-VIS-NIR absorption spectra of the unmodified SnO_2 and CuO-loaded SnO_2 (CuO/SnO_2). The unmodified SnO_2 exhibits the UV absorption due to the interband transition (band gap = 3.6 eV). In addition, the strong absorption is obserbed in the NIR region (> 900 nm). Since the SnO_2 calcination in air weakens the NIR absorption, the absorption could be derived from the free carriers by the oxgen vacancy.[29] The surface modification of SnO_2 with CuO causes a red-shift in the absorption edge. Also, the absorption around 800 nm due to the d-d transition of Cu^{2+} ions intensifies,[30] also indicating that the oxidation number of copper ions is +2.

To confirm the morphology of CuO on the SnO_2 surface, CuO/SnO particles were observed by TEM. Fig. 3a shows a TEM image of the CuO/SnO_2 particles with Γ = 1.83. No particulate deposits are observed on the SnO_2 surface in spite that 0.2 mass% Cu is loaded on it. At the first step in the CCC technique, $Cu(acac)_2$ is strongly adsorbed on the surface by chemisorption, and the adsorbed species are spatially separated by the bulky acac-ligands. Consequently, in the calcination at the second step, the aggregation of the oxidized species is suppressed, and very small oxide clusters can be generated. We have recently showed by extended X-ray absorption fine structure (EXAFS) spectroscopy that isolated Fe_2O_3 clusters are formed on the TiO_2 surface by the CCC technique.[25,28] Thus, CuO could also be present on the surface as molecular scale clusters. By the same way as the preparation of Au/mp-TiO_2, a CuO/SnO_2 paste layer (thickness ≈ 25 μm and area = 4 cm^2) was coated on FTO by the doctor blade technique, and the post-heating in air at 500 °C for 1 h yielded a mesoporous CuO/mp-SnO_2 film on FTO (CuO/mp-SnO_2 | FTO). Fig. 3b shows a SEM image for the cross-section of CuO/mp-SnO_2(apparent surface area, S_a = 4 cm^2) | FTO. A CuO/mp-SnO_2 film with thickness of ~5 μm is formed on the FTO film. Also, the mp-Au/TiO_2 film (S_a = 16 cm^2) was partly pre-coated on the surface of FTO (S_a = 24 cm^2), and then, the CuO/mp-SnO_2 film was formed on the left FTO part (S_a = 8 cm^2) to yield Au/mp-TiO_2(S_a = 16 cm^2) | FTO | CuO/mp-SnO_2(S_a = 8 cm^2). Further, top-down SEM images and the energy dispersive X-ray (EDX) analysis for the Au/mp-TiO_2 and the CuO/mp-SnO_2

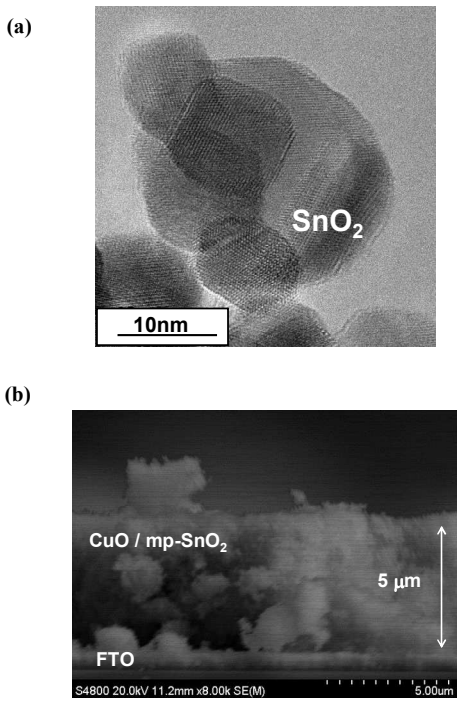

Fig. 3. (a) TEM image of as-prepared CuO/SnO_2 particle with Γ = 1.83. (b) Cross-sectional SEM image of CuO/mp-SnO_2.

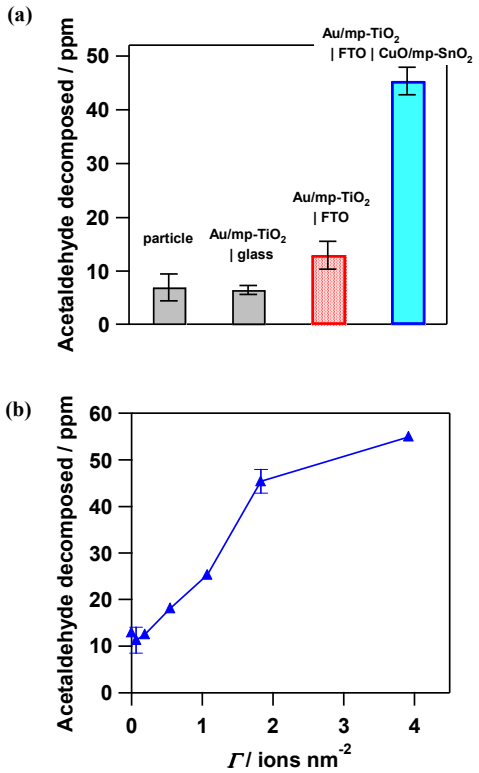

Fig. 4. (a) Decomposed amount of acetaldehyde at reaction time = 24 h. (b) Plots of decomposed amount of acetaldehyde as a function of Γ.

parts in the bi-overlayer type photocatalyst confirm that Au and Cu are present in the Au/mp-TiO_2 and CuO/mp-SnO_2 regions, respectively, exclusively each other (Fig. S3 in ESI).

3.3 Photocatalytic decomposition of gaseous acetaldehyde

As a gas-phase test reaction, degradation of gaseous acetaldehyde was carried out to evaluate the photocatalytic activity of the Au/mp-TiO_2(S_a = 16 cm^2) | FTO | CuO/mp-SnO_2(S_a = 8 cm^2), Au/TiO_2 particles (16 mg), Au/mp-TiO_2(S_a = 16 cm^2) | FTO, and Au/mp-TiO_2(S_a = 16 cm^2) | glass. In this case, since Au/mp-TiO_2(S_a = 1 cm^2) is comprised of ~ 1 mg of Au/TiO_2 particles, 16 mg of Au/TiO_2 particles was used for comarison. A reaction chamber (0.64 L) with catalyst placed was evacuated by a rotary vacuum pump. Then, a nitrogen-balanced acetaldehyde gas (516 ppm) was introduced to be diluted to ~100 ppm with ambient air, and the resulting relative humidity in the reaction chamber was ~ 30%. After 2 h exposure in the dark, visible-light (λ > 430 nm) was irradiated for 24 h. Fig. 4a compares the visible-light activities of the four photocatalysts for the acetaldehyde degradation. The activity of Au/mp-TiO_2 | FTO is significantly higer than those of the Au/TiO_2 particle and Au/mp-TiO_2 | glass. This result is ascribable to the efficient charge separation in Au/mp-TiO_2 | FTO as reported in our preceding paper.[23] Interestingly, Au/mp-TiO_2 | FTO | CuO/mp-SnO_2 (Γ = 1.83) exhibits an activity far exceeding that of Au/mp-TiO_2 | FTO, and the activity is ~6 times larger than the particle system. Further, 17 ppm of CO_2 was generated at 2 h. The activity

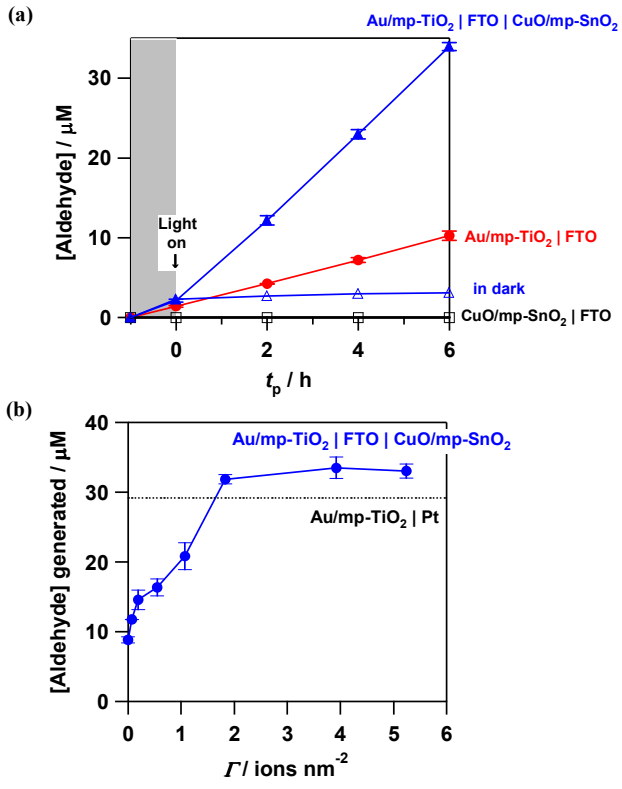

Fig. 5. (a) Time courses for cinnamyl alcohol oxidation by Au/mp-TiO_2 | FTO | CuO/mp-SnO_2 (Γ = 1.83) and Au/mp-TiO_2 | FTO. (b) Plots of amount of aldehyde generated after 6 h illumination as a function of Γ.

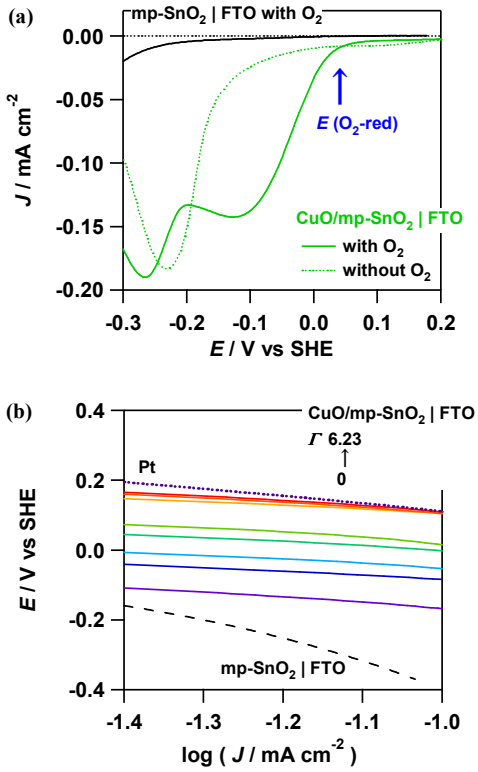

Fig. 6. (a) Dark current density (J)-potential (E) curves of CuO/mp-SnO_2 (Γ = 0.55) and mp-SnO_2 electrode measured in 0.1 M $NaClO_4$ solutions under aerated and deaerated conditions. (b) Tafel plots of the dark current (J)-potential (E) curves around O_2-reduction region for the CuO/mp-SnO_2/FTO with varying Γ.

enhancement by CuO/mp-SnO_2 depends on the CuO-loading amount Γ. Fig. 4b shows the degradation amounts of acetaldehyde as a function of Γ. The amount remarkably increases with increasing Γ.

3.4 Photocatalytic selective oxidation of cinnamyl alcohol

As a liquid-phase test reaction, the oxidation of cinnamyl alcohol was carried out to study the effect of CuO/mp-SnO_2 on the visible-light activity. Visible-light irradiation (λ > 430 nm) of Au/mp-TiO_2(S_a = 4 cm^2) | FTO | CuO/mp-SnO_2(S_a = 4 cm^2, Γ = 1.83) and Au/mp-TiO_2(S_a = 4 cm^2) | FTO selectively oxidized cinnamyl alcohol to cinnamaldehyde.[12,13] Fig. 5a shows time courses for the cinnamaldehyde generation in the dark and under visible-light irradiation. The oxidation of cinnamyl alcohol occurs even in the dark to be sluggish after 1 h because the thermocatalytic activity of the large Au particle (d = 6.9 nm) is low.[31] Under visible-light irrdiation, the reaction proceeds apparently with the zero-order rate law obeyed, whereas CuO/mp-SnO_2 (Γ = 1.83) | FTO is inactive. The rate constant for Au/mp-TiO_2 | FTO | CuO/mp-SnO_2 (Γ = 1.83) (5.3 μM h^{-1}) is greater than that for Au/mp-TiO_2 | FTO (1.5 μM h^{-1}) by a factor of 3.6. Thus, loading of CuO/mp-SnO_2 is also effective in the liquid-phase reaction. Fig. 5b shows the amount of aldehyde generated after 6 h illumination as a function of Γ. The aldehyde amount increases with increasing Γ, and reaches constant at Γ > 2. It is noteworthy that the amount at Γ > 2 is larger than that for the

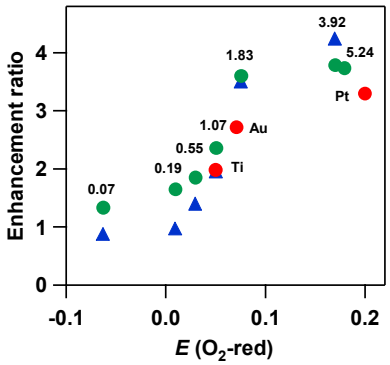

Fig. 7. Plots of enhancement ratio for acetaldehyde decomposition (blue, triangle) and selective alcohol oxidation (green and red, circle) as a function of the $E(O_2\text{-red})$ value for the CuO/mp-SnO_2 | FTO. The number shows Γ, and Pt, Au, Ti denote the data for Au/mp-TiO_2 | Pt, Au/mp-TiO_2 | Au, and Au/mp-TiO_2 | Ti, respectively.

Au/mp-TiO_2 | Pt system.[23]

3.5 Electrocatalysis of CuO/SnO_2 for oxygen reduction

To clarify the effect of CuO/mp-SnO_2 | FTO on the visible-light activity of the bi-overlayer type photocatalyt, the electrocatalytic acitivity of CuO/mp-SnO_2 | FTO for ORR was examined. Fig. 6a shows the dark current (J)-potential (E) curves for CuO/mp-SnO_2(S_a = 4 cm^2) | FTO (Γ = 0.55) and mp-SnO_2(S_a = 4 cm^2) | FTO without CuO loading under deaerated and aerated conditions. For the mp-SnO_2 | FTO electrode, the reduction current is very small at E < -0.3 V vs. standard hydrogen electrode (SHE) in the absence and presence of O_2. Under deaerated conditions, CuO/mp-SnO_2 | FTO shows a reduction peak at -0.25 V vs. SHE, which can be assigned to the reduction of CuO.[32] Under aerated conditions, a large current due to O_2 reduction is observed at E < +0.03 V vs. SHE. Clearly, CuO clusters on the SnO_2 surface have an electrocatalytic activity for O_2 reduction. As an indicator for the electrocatalytic activity, the onset-potential of the O_2 reduction current ($E(O_2\text{-red})$) is employed. Fig. 6b shows the Tafel plots for the J-E curves around the potential region where the O_2 reduction occurs for the CuO/mp-SnO_2 | FTO with varying Γ. Whereas the Tafel slope is almost constant irrespective of Γ, the overpotential (η) decreases with increasing Γ and the η values of the samples with Γ > 3.9 are comparable to that of Pt film. This finding indicates the possibility of the CuO/mp-SnO_2 for the application to the various ORR-devices.

The enhancement ratio of the photocatalytic reaction was defined as the ratio of the visible-light activity of Au/mp-TiO_2 | FTO | CuO/mp-SnO_2 to that of Au/mp-TiO_2 | FTO. Fig. 7 shows the relationship between the $E(O_2\text{-red})$ value and the enhancement ratios for the two photocatalytic reactions, i.e. acetaldehyde decomposition and alcohol oxidation. A good positive correlation between the enhancement ratios and the $E(O_2\text{-red})$ value is observed, and the enhancement factors in the acetaldehyde decomposition and the cinnamylalcohol oxidation increase with an increase in Γ at Γ < 3.92 and Γ < 5.24, respectively. Thus, the electrocatalytic activity of CuO/mp-SnO_2 for the O_2 reduction is the major factor governing the visible-light activity of the Au/mp-TiO_2 | FTO | CuO/mp-SnO_2-type "plasmonic photocatalyst". A closer inspection indicates that the activity for ORR monotonously increases with increasing CuO-coverage at Γ < 5.24, which is parallel to the photocatalytic activity for the acetaldehyde decomposition. However, the photocatalytic activity for the cinnamyl alcohol oxidation is saturated at Γ > 1.83. At the high CuO-coverage region, the photocatalytic activity could be limited by the diffusion of cinnamyl alcohol to the catalyst surface since the diffusion in liquid-phase is generally much slower than that in gas-phase.

3.6 Essential mechanism

The basic action mechanism on the present bi-overlayer type

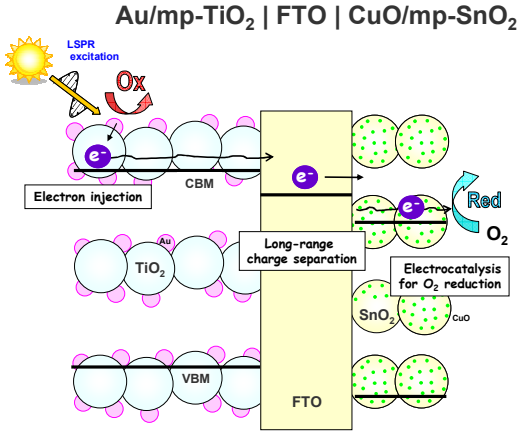

Scheme 2. Proposed action mechanism for bi-overlayer type plasmonic photocatalysts.

"plasmonic photocatalyst" can be summarized as Scheme 2. Visible-light irradiation excites the LSPR of Au nanoparticles on TiO_2. The electrons are injected into to the CB(TiO_2)[7,8] further to the FTO underlayer, which is energetically possible.[33] The electrons further move to the CuO clusters through the conducting FTO and mp-SnO_2 films. The long-rage charge separation is achieved by the electron transport (Au → TiO_2 → FTO, SnO_2 → CuO). As a result, O_2 is efficiently reduced with the assistance by the excellent electrocatalytic activity for ORR of the CuO clusters. On the other hand, the effective lowering in the Fermi energy of Au nanoparticles causes oxidation of organic reactants on their surfaces. Also, the mesoporous structures of the Au/TiO_2 and CuO/SnO_2 films are very important in that they permit the the permeation of the reaction solution into the pores, consequently, a gerat number of active sites are available for the reactions. On the other hand, the electron transport among nanosized domains is well known to be not very efficient.[34-36]The solution to this problem allows us to expect further improvement in the photocatalytic activity of the present bi-overlayer plasmonic photocatalyst.

4 Conclusions

This study has shown that a Au/mp-TiO_2 | CuO/mp-SnO_2 bi-overlayer type "plasmonic photocatalyst" formed on the FTO substrate exhibits a high level of visible-light activity for the gas-phase and liquid-phase reactions. This study would present a new design for the highly active and practical visible-light photocatalysts. Also, CuO/mp-SnO_2 can be anticipated as the key component for the various ORR-devices.

Acknowledgements

TAYCA Co. kindly gifted us with MT-700B. This work was partially supported by a Grant-in-Aid for Scientific Research (C) No. 24550239 and MEXT-Supported Program for the Strategic Research Foundation at Private Universities.

Notes and references

[a] *Environmental Research Laboratory, Kinki University, 3-4-1, Kowakae, Higashi-Osaka, Osaka 577-8502, Japan.*
[b] *Department of Applied Chemistry, School of Science and Engineering, Kinki University, 3-4-1, Kowakae, Higashi-Osaka, Osaka 577-8502, Japan.*

† Electronic Supplementary Information (ESI) available: [TEM image of as-prepared Au/TiO_2 particle and Au particle size distribution. Cross-sectional SEM image of Au/mp-TiO_2 and UV-Vis absorption spectra. Top-down SEM images and EDX spectra of bi-overlayer type plasmonic photocatalysts.]. See DOI: 10.1039/b000000x/

‡ Footnotes should appear here. These might include comments relevant to but not central to the matter under discussion, limited experimental and spectral data, and crystallographic data.

1 U. Kreibig and M. Vollmer, *Optical Properties of Metal Clusters*. Springer: Berlin, 1995.
2 C. F. Bohren and D. R. Huffman, *Absorption and Scattering of Light by Small Particles*. Wiley: New York, 1983.
3 G. V. Hartland, *Chem. Rev.,* 2011, **111**, 3858-3887.
4 A. Kubacka, M. Fernandez-Garcia, and G. Colon, *Chem. Rev.*, 2012, **112**, 1555-1614.
5 K. Ueno and H. Misawa, *J. Photochem. Photobiol. C: Photochem. Rev.,* 2013, **15**, 31-52.
6 X. Lang, X. Chen, and J. Zhao, *Chem. Soc. Rev.,* 2014, **43**, 473-486.
7 Y. Tian and T. Tatsuma, *J. Am. Chem. Soc.,* 2005, **127**, 7632-7637.
8 A. Furube, L. Du, K. Hara, R. Katoh and M. Tachiya, *J. Am. Chem. Soc.,* 2007, **129**, 14852-14853.
9 E. Kowalska, Z. Wei, B. Karabiyik, M. Janczarek, M. Endo, K. Wang, P. Rokicka, A. Markowska-Szczupak, and B. Ohtani, *Adv. Sci. Tech*., 2014, **93**, 174-183.
10 S. Naya, T. Nikawa, K. Kimura, and H. Tada, *ACS Catal.,* 2013, **3**, 903-907.
11 E. Kowalska, R. Abe, and B. Ohtani, *Chem. Commun.,* **2009**, 241-243.
12 S. Naya, A. Inoue, and H. Tada, *J. Am. Chem. Soc.,* 2010, **132**, 6292-6293.
13 K. Kimura, S. Naya, Y. Jin-nouchi, and H. Tada, *J. Phys. Chem. C,* 2012, **116**, 7111-7117.
14 D. Tsukamoto, Y. Shiraishi, Y. Sugano, S. Ichikawa, S.; Tanaka, and T. Hirai, *J. Am. Chem. Soc.,* 2012, **134**, 6309-6315.
15 S. Naya, S.; M. Teranishi, T. Isobe, and H. Tada, *Chem. Commun.,* 2010, **46**, 815-817.
16 Y. Ide, M. Matsuoka, and M. Ogawa, *J. Am. Chem. Soc.,* 2010, **132**, 16762-16764.
17 Z. Zheng, B. Huang, X. Qin, X. Zhang, Y. Dai, J. Wei, and M.-H. Whangbo, *J. Mater. Chem.,* 2011, **21**, 9079-9087.
18 S. Naya, K. Kimura, and H. Tada, *ACS Catal.,* 2013, **3**, 10-13.
19 L. Du, A. Furube, K. Yamamoto, K. Hara, R. Katoh, and M. Tachiya, *J. Phys. Chem. C,* 2009, **113**, 6454-6462.
20 S. Naya, T. Niwa, T. Kume, and H. Tada, *Angew. Chem. Int. Ed.,* 2014, **53**, 7305-7309.
21 Y. Ide, F. Liu, J. Zhang, N. Kawamoto, N. Komaguchi, Y. Bando, and D. Golberg, *J. Mater. Chem. A,* 2014, **2**, 4150-4156.
22 Z. Bian, T. Tachikawa, P. Zhang, M. Fujitsuka, and T. Majima, *J. Am. Chem. Soc.,* 2014, **136**, 458-465.
23 T. Kume, S. Naya, and H. Tada, *J. Phys. Chem. C,* 2014, **118**, 26887-26893.
24 J. Wu and H. Yang, *Acc. Chem. Res.,* 2013, **46**, 1848-1857.
25 Q. Jin, M. Fujishima, A. Iwaszuk, M. Nolan, and H. Tada, *J. Phys. Chem. C,* 2013, **117**, 23848-23857.
26 S. Tsubota, M. Haruta, T. Kobayashi, A. Ueda, and Y. Nakahara, *Preparation of Catalysis V*. Elsevier, Amsterdam, **1991**.
27 H. Tada, T. Kiyonaga, and S. Naya, *Metal Oxide-Supported Gold Nanoparticles*, Lambert Academic Publishing, **2012**.
28 H. Tada, Q. Jin, H. Nishijima, H. Yamamoto, M. Fujishima, S. Okuoka, T. Hattori, Y. Sumida, and H. Kobayashi, *Angew. Chem. Int. Ed.,* 2011, **50**, 3501-3505.
29 B. Ouni, A. Boukhachem, S. Dabbous, A. Amlouk K. Boubaker, and M. Amlouk, *Mater. Sci. Semiconductor Process*. 2010, **13**, 281.
30 H. Irie, K. Kamiya, T. Shibanuma, S. Miura, D. A. Tryk, T. Yokoyama, and K. Hashimoto, *J. Phys. Chem. C,* 2009, **113**, 10761-10766.
31 H. Tsunoyama, N. Ichikuni, H. Sakurai, and T. Tsukuda, *J. Am. Chem. Soc.,* 2009, **131**, 7086-7093.
32 S. Nakayama, T. Kaji, T. Notoya, and T. Osakai, *Electrochimica Acta,* 2008, **53**, 3493-3499.
33 H. Tada, A. Hattori, Y. Tokihisa, K. Imai, N. Tohge, and S. Ito, *J. Phys. Chem. B,* 2000, **104**, 4585-4587.
34 J. Lee, S. Mubeen, X. Ji, G. D. Stucky, and M. Moskovits, *Nano Lett.,* 2012, **12**, 5014-5019.
35 S. Mubeen, J. Lee, N. Singh, S. Krämer, G. D. Stucky, and M. Moskovits, *Nat. Nanotechnol.,* 2013, **8**, 247-251.
36 S. Mubeen, J. Lee, W-R, Lee, N. Singh, G. D. Stucky, and M. Moskovits, *ACS Nano*, 2014, **8**, 6066-6073.